Angle-resolved photoemission study of clean and hydrogen-saturated Mo(110)

Jörg Kröger, Thomas Greber, and Jürg Osterwalder
Physik-Institut der Universität Zürich, Winterthurerstraße 190, 8057 Zürich, Switzerland
(Received 28 September 1999; revised manuscript received 23 December 1999)

We present the development of Fermi-level crossings from the clean to the hydrogen-saturated (110) surface of molybdenum at room temperature. The well-known adsorbate-induced phonon anomaly is discussed in terms of a quasi-one-dimensional Fermi-surface nesting and giant Kohn anomaly. Our experiment resolved an existing discrepancy between earlier photoemission data and Fermi-surface contours calculated within density-functional theory. Moreover, it is found that the Fermi-surface nesting is fully established at hydrogen coverages where the phonon anomaly just barely forms.

I. INTRODUCTION

The coupling of electronic and nuclear degrees of freedom, i.e., the breakdown of the adiabatic approximation, belongs to the very base of solid-state physics and can lead to fascinating effects, such as reconstruction or anomalous phonon softening. Often, the interaction of electrons and ions goes hand in hand with a reduction of the dimensionality of the system under investigation. This phenomenon will now be illustrated with the aid of subsequent examples covering both experimental and theoretical results on molybdenum crystals. Using the inelastic scattering of neutrons Powell, Martell, and Woods[1] show that phonon energies at H and N of the first Brillouin zone are anomalously low. Varma and Weber[2,3] interpret the lowering of the phonon modes as a consequence of lattice instabilities. They realize that the perturbation of the lattice periodicity depends on the existence of electronic states close to the Fermi level. These electronic states are among Fermi-surface contours that have large parts of matching curvature. In the literature this situation is called *quasi-one-dimensional Fermi-surface nesting* in order to emphasize the similarity to the one-dimensional case where the Fermi surface consists of two parallel planes. This is the reduction of the dimensionality mentioned above. Varma and Weber point out that the wave vectors of the anomalous phonon modes equal the vectors spanning the nested regions of the Fermi contours. Additional measurements for the H-point anomaly[4] demonstrate that the lowering of the phonon energy decreases with increasing temperature. Thus it is proved experimentally that electronic states close to the Fermi level are responsible for the phonon anomaly. By means of the *frozen phonon method* the frequencies of the phonon modes at H and N could be reproduced theoretically.[5–9] The introduced phonon anomalies at H and N may be called *intrinsic* because they exist *a priori*.

The reconstruction of the clean (100) surface of molybdenum serves as an example for what might be called a *temperature-induced* phonon anomaly. Investigations by means of low-energy electron diffraction for Mo(100) reveal a reversible structural transformation which depends on the surface temperature.[10,11] For temperatures $T>T_c\approx 250\,\mathrm{K}$ the common (1×1) diffraction pattern is observed. For values below the critical temperature T_c, however, a quartet of diffraction spots around the $(\frac{1}{2}\frac{1}{2})$ position is monitored. Felter, Barker, and Estrup[11] postulate that this phenomenon is characteristic for the clean surface and is due to a periodic translation of surface atoms. Interestingly, using the inelastic scattering of helium atoms Hulpke and Smilgies discover that the energy of a phonon mode along [110] decreases to zero.[12] This indentation in the dispersion curve of the corresponding phonon mode is localized at a wave vector which is in agreement with the reciprocal-lattice vector of the mentioned periodic lattice perturbation. Combining the results of the low-energy electron diffraction experiment and the vibrational spectroscopy the following picture is conveyed: a still unknown mechanism freezes a soft phonon of vanishing energy and thus causes a static and periodic change of the lattice constant which leads to the observed diffraction pattern. A hint for the underlying mechanism is furnished by measurements using angle-resolved photoemission spectroscopy.[13] The authors present Fermi contours of electronic surface states and claim that decreasing the temperature starting with values $T>T_c$ causes a change from convex to concave curvature of the contours. Especially at T_c the curvature is extremely flat which produces significant nesting features. Again the nesting vector, i.e., the reciprocal vector spanning the nested contours, compares well with the wave vector of the anomalous phonon mode.

The last example is dedicated to Mo(110). By means of a He atom scattering experiment examining the clean and hydrogen-saturated surface in terms of surface phonons Hulpke and Lüdecke find that the dispersion of both the transversal and the longitudinal acoustic-phonon modes, which will be referred to as the Rayleigh wave and the longitudinal mode, respectively, are extraordinary. They observe that beginning from $\approx 0.6\ \mathrm{Å}^{-1}$ along the $\overline{\Gamma N}$ direction towards the boundary of the surface Brillouin zone the energy of the longitudinal mode is lowered.[14–16] The dispersion curves for the hydrogen-saturated surface reveal two anomalous branches for the Rayleigh wave along [001] (see Fig. 1 for a definition of the directions of the direct and the reciprocal lattice). Two indentations of different magnitude of the dispersion curve are found at a wave vector of $\approx 0.9\ \mathrm{Å}^{-1}$. Compared to the clean surface the energy of the Rayleigh wave is lowered from $\approx$17 to $\approx$14 meV and from $\approx$17 to $\approx$2.5 meV for the small and the deep indentation, respectively. Also at the $\overline{S}$ point of the surface Brillouin zone cor-

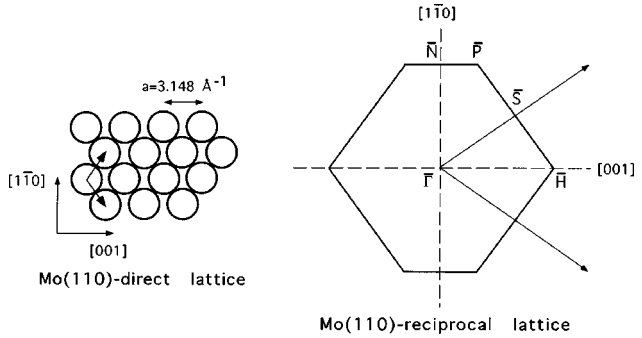

FIG. 1. Direct and reciprocal lattice of Mo(110). Symmetry directions and high symmetry points of the surface Brillouin zone are defined.

responding to a wave vector of ≈ 1.2 Å^{-1} along $[1\bar{1}2]$ an indentation of the dispersion curve of the Rayleigh wave down to ≈ 11 meV is detected. Rotating the crystal azimuthally and thus changing the momentum transfer of the He atoms the authors find that the anomaly becomes only slightly weaker for wave vectors whose orthogonal projection onto [001] remains ≈ 0.9 Å^{-1}. Thus they postulate a quasi-one-dimensional character of the observed phonon anomaly. Moreover, using deuterium as the adsorbate the anomaly remains unchanged and it becomes clear that the anomalous behavior of surface phonons is driven by the chemical nature of the adsorbate and not, for instance, by its mass.

An equivalent experiment using the inelastic scattering of electrons, i.e., electron-energy-loss spectroscopy, essentially leads to the same results.[17,18] While the deep indentation in the dispersion curves could not be observed, which is due to the different scattering mechanisms, it is shown that also the longitudinal mode reveals an anomalous lowering of its energy at the discussed critical wave vectors. Furthermore, it is pointed out that the anomaly becomes less in magnitude with increasing temperature. At room temperature the anomaly for both phonon modes is still clearly visible. Finally the authors find that the anomaly grows in for coverages below saturation (see Fig. 2 for a representation of the surface phonon dispersion curves).

Both clean and hydrogen-saturated Mo(110) surfaces have also been investigated by means of angle-resolved photoelectron spectroscopy.[19–24] The results are summarized in the right column of Fig. 3. Here the Fermi-surface contours for surface states and surface resonances are shown for the clean surface (upper part) and for the hydrogen-saturated system. The shaded areas are bulk electronic states that are projected onto the (110) surface. The crosses mark locations where a surface state or a surface resonance crosses the Fermi level. Around $\bar{\Gamma}$, $\bar{N}$, and $\bar{S}$ (see Fig. 1 for a definition of the symmetry points of the surface Brillouin zone) *hole pockets* are located, i.e., contours that enclose unpopulated states. An *electron pocket*, i.e., a contour that encloses populated states, is visible along the $\bar{\Gamma}\bar{N}$ direction. Now Jeong, Gaylord, and Kevan find that with hydrogen adsorption the hole pockets become smaller and vanish at saturation.[24] Simultaneously the electron pocket grows in area, i.e., the energies of the electronic states are lowered with respect to the Fermi energy. At saturation this contour coalesces with the corresponding contour of the second surface Brillouin zone and thus new hole pockets around $\bar{N}$ and $\bar{S}$ are fully developed [Fig. 3(d)]. As is obvious from the figure these hole pockets are situated predominantly in the projected band gap that unambiguously characterizes them as surface states. The authors extract reciprocal vectors which should enable quasi-one-dimensional Fermi-surface nesting and thus should drive the giant Kohn anomaly (see Table I, third column).

The left-hand side of Fig. 3 displays theoretical results based on density-functional theory using the full-potential linearized augmented plane-waves method.[25–28] Concerning the clean case the calculations can reproduce the experimental findings in good agreement. Kohler *et al.* state that the identified bands are extremely localized at the surface and that they are of *d* character. Specifically, the contour of the electron pocket is due to a $(d_{3z^2-r^2}, d_{xy})$ band.[25–28] The results for the hydrogen-saturated surface, however, differ significantly. Following the theoretical results it is obvious that the $(d_{3z^2-r^2}, d_{xy})$ band is shifted along the $\bar{\Gamma}\bar{H}$ direction towards the projected band gap. The authors emphasize that this shift is not due to a hybridization of the hydrogen orbitals with the corresponding surface band but a consequence of a modification of the surface potential. It is important to note that the $(d_{3z^2-r^2}, d_{xy})$ states lose their three-dimensional character and become pure two-dimensional surface states. Another reduction of the dimensionality is obtained by the development of nested regions of the calculated Fermi contours. According to the results of Kohler *et al.* the extracted nesting vectors (see Table I, first column) are in good agreement with the wave vectors of the anomalous phonon modes (Table I, second column). The discussed discrepancy between theory and the photoemission experiment was the main impetus for us to perform our experiment.

Let us finally comment briefly on hydrogen coverages and ordered adsorbate structures on Mo(110). It is known from structure analysis by means of low-energy electron diffraction[29–32] and from electron-energy-loss spectroscopy[17,18] that hydrogen is adsorbed atomically in the threefold-coordinated hollow site for all coverages. Experiments using low-energy electron diffraction find that at 0.5-ML hydrogen coverage a (2×2)2H superstructure with two hydrogen atoms per adsorbate unit cell exists which is combined with a slight rippling of the surface.[31] The (1×1) diffraction pattern is restored for the hydrogen-saturated surface at 1 ML. An electron-energy-loss spectroscopy experiment reports another adsorbate superstructure for a coverage of 0.75 ML.[17,18] While the diffraction pattern remains a (2×2) the specular energy-loss spectra clearly change. Thus an additional (2×2)3H adsorbate superstructure with three hydrogen atoms in the adsorbate unit cell is manifest.

II. EXPERIMENTAL

For the experiment we use the (110) surface of a molybdenum single crystal. Molybdenum crystallizes in the body-centered-cubic structure with a lattice constant of $a = 3.148$ Å. The surface has been cut and polished to within 0.3° of the desired orientation. Before the crystal was installed into the ultrahigh vacuum chamber it was heated to 1300 K in a hydrogen atmosphere for several hours.

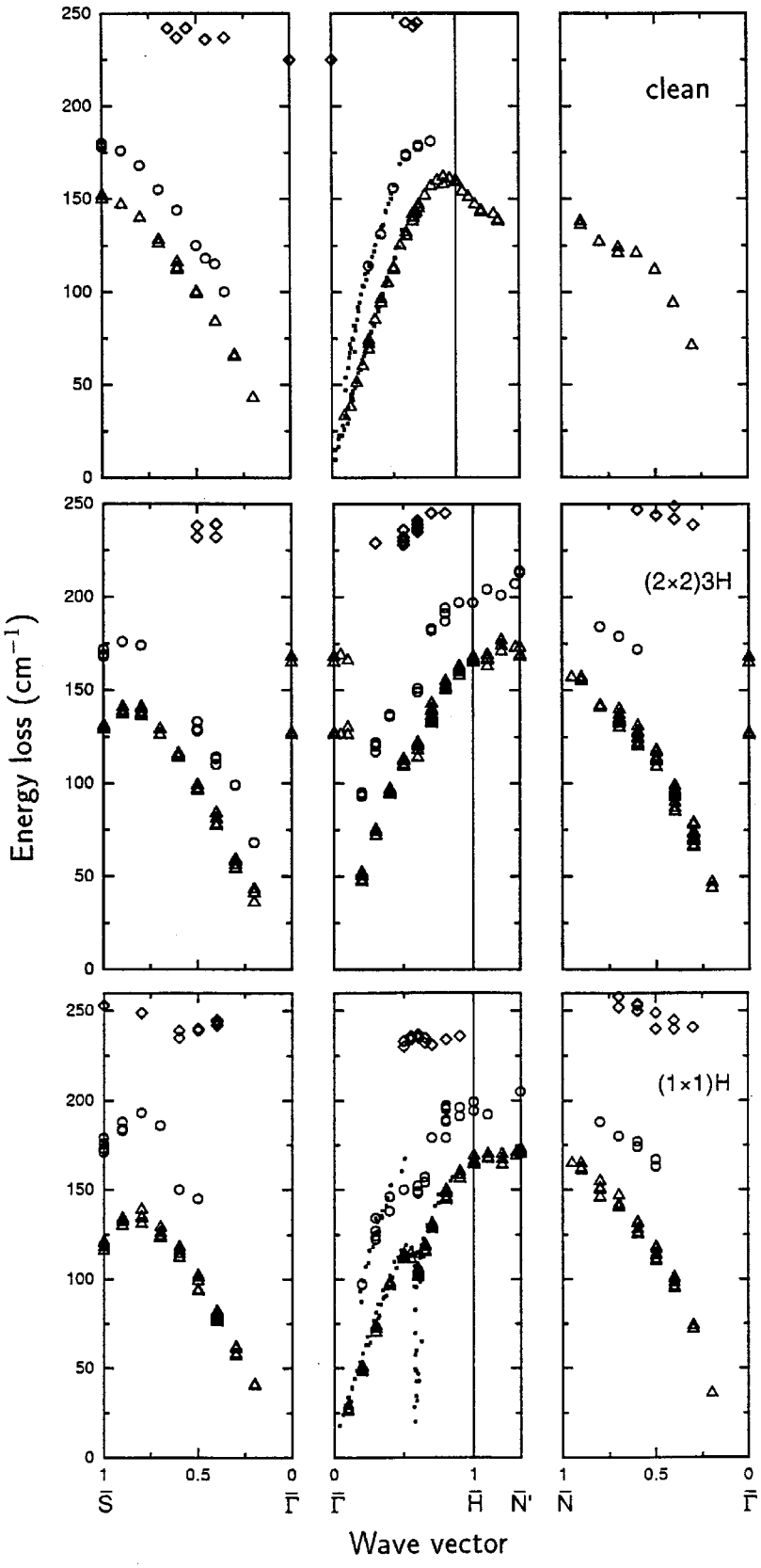

FIG. 2. Summary of the dispersion curves for the Rayleigh wave (triangles) and the longitudinal mode (circles) for the main symmetry directions of the surface Brillouin zone as defined in Fig. 1. The dispersion of the phonon modes was recorded for the clean surface (upper data sets), the (2×2)3H phase at 0.75 ML, and the hydrogen-saturated surface $[(1\times1)\mathrm{H}]$ at 1 ML coverage. The phonon wave vectors are given in units of the lengths between $\bar{\Gamma}$ and $\bar{H}$, $\bar{S}$, and $\bar{N}$, where $1\ \overline{\Gamma H}=\frac{3}{2}\pi/a$, $1\ \overline{\Gamma S}=\sqrt{\frac{3}{2}\pi/a}$, and $1\ \overline{\Gamma N}=\sqrt{2}\pi/a$. The energy loss of the phonon modes is measured in units of cm^{-1}, where $1\ \mathrm{cm}^{-1}\approx0.124$ meV. Notice that in both the top and the bottom data set for the $\overline{\Gamma H}$ direction results of the analogous He atom scattering experiment are included as small dots (data taken from Ref. 17).

The cleaning procedure as modeled after Refs. 24 and 29 consists of several oxidation cycles where the crystal, being constantly heated to 1400 K, is exposed to oxygen for 10 min and is left without oxygen for 10 min. The oxygen pressure is chosen to be 4×10^{-6} Pa. After accomplishing three cycles the crystal is flashed to 2000 K. This procedure, if necessary, can be repeated several times without degradation of the surface. The flash temperature is achieved by electron bombardment of the back side of the crystal and has been checked using a pyrometer. Having obtained a clean surface after several oxidation cycles it is sufficient to apply only a flash. Surface cleanliness was monitored by low-energy elec-

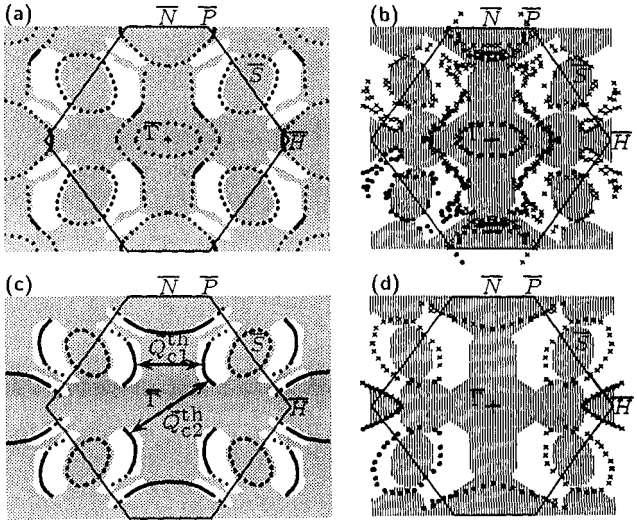

FIG. 3. Comparison between theoretical and experimental results for the Fermi surface of surface states for clean and hydrogen-saturated Mo(110). The left column shows the results obtained by density-functional theory calculations (Ref. 25); the right column displays the results as obtained by a previous photoemission experiment (Refs. 22 and 23).

tron diffraction, x-ray photoelectron spectroscopy using Mg $K\alpha$ radiation, and ultraviolet photoelectron spectroscopy. The reader is referred to Fig. 4(a) for the energy distribution curve of the clean surface in normal emission. This spectrum has also been observed by Jeong, Gaylord, and Kevan[24] near normal emission. The authors assign the peak at $\approx$1.4 eV to be a spin-orbit-induced surface resonance. Also shown is the energy distribution curve after $\approx$90 min in ultrahigh vacuum with a base pressure of less than 1×10^{-8} Pa. There are two obvious changes: firstly, a broad spectral feature at $\approx$4.9 eV for the clean surface shifts to $\approx$4.2 eV; secondly, the spin-orbit-induced surface resonance peak decreases its intensity by $\approx$30% with respect to the clean surface and shifts slightly to a higher binding energy. For us it is important that the Fermi edge is not affected during the 90 min that follows from recording energy distribution curves every 90 s. The proof of good local atomic order has been given by x-ray photoelectron diffraction which allowed for determining the crystal orientation and the main symmetry axis to within an accuracy of less than 1° (see Fig. 5).

TABLE I. Critical wave vectors for the anomalous phonon modes as obtained theoretically by density-functional theory [(DFT) (Refs. 25–28)] and experimentally by electron-energy-loss spectroscopy [(EELS) (Refs. 17 and 18)] and photoelectron spectroscopy [(PES) (Ref. 23)]. Notice the significant difference between theory and the photoemission experiment for both symmetry directions. The last column is dedicated to our own results where very good agreement with both theory and the EELS experiment is revealed.

	$\lvert\mathbf{Q}_c^{\text{theo}}\rvert$ (DFT) (Å^{-1})	$\lvert\mathbf{Q}_c^{\text{exp}}\rvert$ (EELS) (Å^{-1})	$\lvert\mathbf{Q}_c^{\text{exp}}\rvert$ (PES) (Å^{-1})	$\lvert\mathbf{Q}_c^{\text{exp}}\rvert$ (PES) (Å^{-1})
$\overline{\Gamma H}([001])$	0.86	0.90	1.31	0.85
$\overline{\Gamma S}([1\bar{1}2])$	1.23	1.22	1.50	1.19

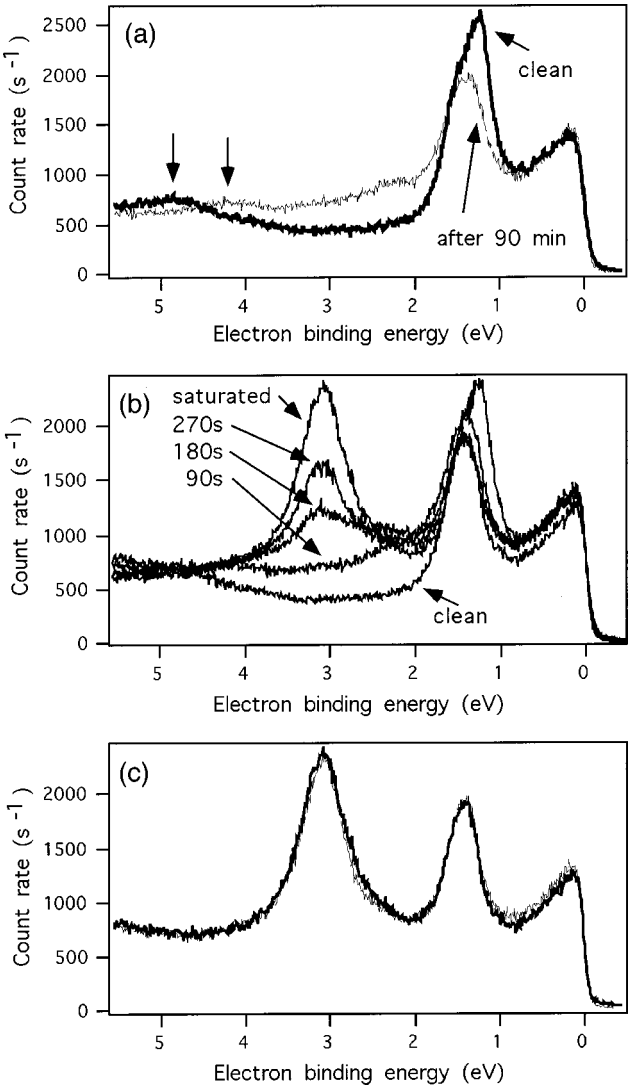

FIG. 4. Energy-distribution curves in normal emission. In (a) the spectrum for the clean surface (bold line) is shown and the effects of residual gas exposure in ultrahigh vacuum after 90 min are demonstrated (thin line). In (b) the development of the spectra with increasing hydrogen exposure is revealed. In (c) the stability of the hydrogen-saturated surface under He *I* radiation is shown. One spectrum was recorded immediately after preparing the saturated surface; the second one was recorded 60 min later.

Hydrogen exposure was performed using gas of 99.995% purity and by backfilling the chamber to 1×10^{-7} Pa for small coverages and 5×10^{-6} Pa for saturating the surface. The crystal was exposed to hydrogen at room temperature and a sensitivity factor of 1.6 for the Bayard-Alpert ion gauge has been taken into account for quantifying the amount of exposure. The development of the normal-emission energy-distribution curves with increasing hydrogen exposure is demonstrated in Fig. 4(b). Starting with the clean surface the crystal is exposed successively to hydrogen for 90 s at a pressure of 1×10^{-7} Pa. The saturated surface corresponds to an exposure for 30 min at 5×10^{-6} Pa. Obviously a peak at $\approx$3.1 eV grows in and increases in intensity with increasing coverage until saturation is reached. Figure

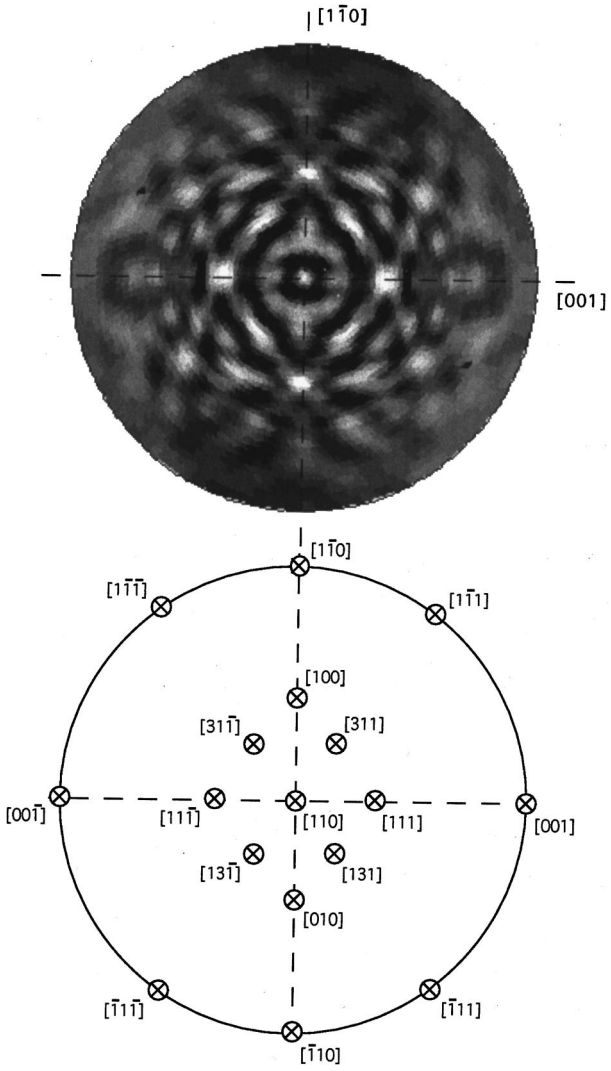

FIG. 5. (a) X-ray photoelectron diffraction pattern of Mo $3d_{3/2}$ ($E_{\mathrm{kin}}=1511.4$ eV) emission from clean Mo(110) at room temperature recorded using Si $K\alpha$ radiation (1739.4 eV). The data are stereographically projected. The outermost data points originate from photoelectrons with nearly grazing emission corresponding to a polar angle of 88°. As the step in the polar angle was chosen to be 2° the total number of data points is 5044. In (b) the most visible spots of (a) are shown and their crystal directions are given.

4(c) compares the energy-distribution curves of a freshly prepared hydrogen-saturated surface with a 60 min older one demonstrating its stability under He I irradiation.

All experiments were carried out in a modified Vacuum Generators Escalab 220 spectrometer.[33] For all ultraviolet photoemission experiments the pass energy of the 180° hemispherical analyzer was set to $E_p=1$ eV in order to achieve an energy resolution of 35 meV full width at half maximum. The iris aperture at the input lens of the analyzer was chosen to get an angular resolution of less than 1° full width at half maximum. The ultraviolet light source is a Gammadata VUV 5000 helium discharge lamp with a toroidal monochromator. For all experiments He $I\alpha$ radiation (21.2 eV) has been used.

Most of the data sets we present in this publication are *Fermi-surface maps*. For this data acquisition mode one out of six channeltron detectors in the analyzer is set to measure photoelectrons precisely from the Fermi energy which has been determined using a polycrystalline Ag sample in a precedent ultraviolet photoemission experiment. Afterwards the sample is rotated both in the polar and in the azimuthal direction in order to collect data points spread uniformly over the hemisphere above the crystal. Thus one is able to measure the complete Fermi surface of surface states covering the whole or parts of the first surface Brillouin zone. The resulting data sets are then presented in a $k_{\parallel}$ projection where $k_{\parallel}$ is the electron momentum component parallel to the surface. Other types of data sets shown here are the angle-scanned energy-distribution curves. Here one fixes the polar or the azimuthal angle and records energy-distribution curves as a function of the varying angle. In both cases, i.e., for Fermi-surface maps and for angle-scanned energy-distribution curves, the data are transformed into a linear gray-scale pattern (for a more detailed discussion of these acquisition modes the reader is referred to Refs. 34 and 35).

III. RESULTS AND DISCUSSION

The strategy of our experiment is as follows: as an overview the complete Fermi-surface maps of both the clean and the hydrogen-saturated surface are desired. After locating the main differences in the Fermi surface contours regions of the first surface Brillouin zone are chosen which allow for a detailed view on the hydrogen-induced changes. These parts of the overall Fermi-surface maps are recorded employing a longer dwell time and an enhanced density of data points with respect to the complete maps.

Figure 6(a) shows the complete Fermi-surface map of clean Mo(110) where the intensity of the photocurrent is presented on a logarithmic scale. Every data point was measured for 1 s and the step in the polar angle was chosen to be 2°, starting at $\theta=50°$, resulting in a total amount of 1898 data points. The concentric circle indicates grazing emission of photoelectrons corresponding to a parallel wave vector $k_{\parallel}=\hbar^{-1}\sqrt{2m(h\nu-E_B-\Phi)}$ (m is the free electron mass, $h\nu$ is the energy of the incident light, E_B is the electron binding energy with respect to the Fermi energy, i.e., $E_B=0.0$ eV at the Fermi surface, $\Phi=4.95$ eV is the work function). Comparing this data set with the results of Jeong, Gaylord, and Kevan[23] [see Fig. 3(b)] we find good agreement. In accordance with their paper we see the hole pockets around $\overline{\Gamma}$, $\overline{N}$, and $\overline{S}$ (we have highlighted these contours by full black lines) which are weak in intensity and the electron pocket elongated along the $\overline{\Gamma N}$ direction ([1$\bar{1}$0], highlighted as a dashed black line) enclosing the $\overline{\Gamma}$ point. In addition, our data set also displays bulk band contributions that happen to cross the Fermi level near the center of the surface Brillouin zone (see for instance Ref. 36), while Jeong, Gaylord, and Kevan[23] concentrated on surface resonances and surface states.

Figure 6(b) is completely analogous to the data set of Fig. 6(a) and displays the Fermi-surface map for the hydrogen-saturated surface. The marked changes in several of the Fermi-surface contours reflect their surface-state character. The contours of the hole pockets have contracted towards their respective high-symmetry points ($\overline{S}$ and $\overline{N}$, see below)

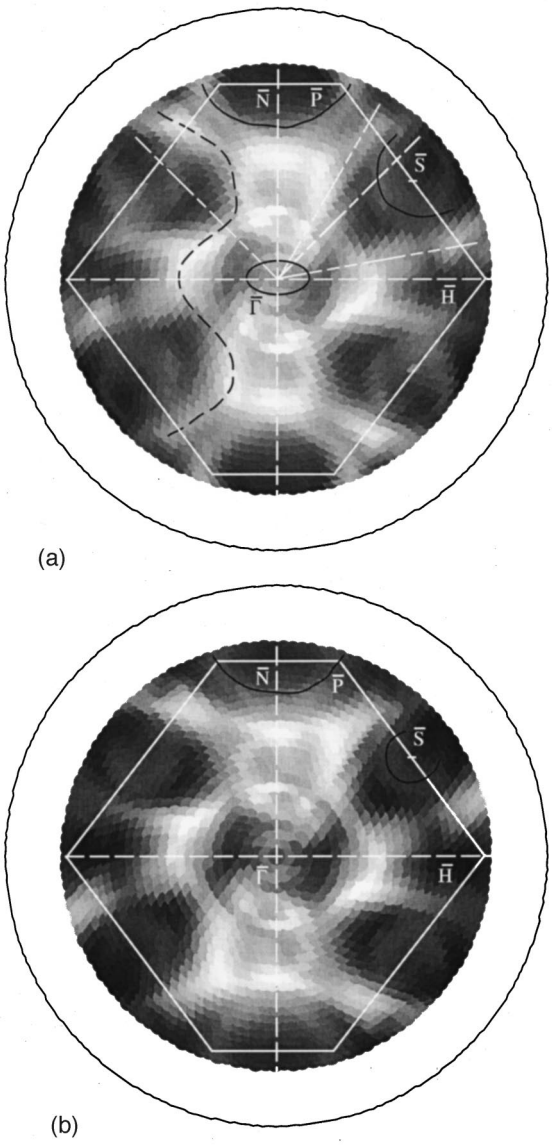

FIG. 6. Complete Fermi-surface map of the clean (a) and the hydrogen-saturated Mo(110) surface. The intensity of the photocurrent is presented on a logarithmic scale. In both data sets we have included the surface Brillouin zone for better orientation. Further, we indicated the regions of the Fermi-surface map that we investigated in greater detail (see the sectors around $\overline{N}$ and $\overline{S}$). In (a) we highlight the hole pockets (full curve) and the electron pocket (dashed line) which were discussed in Ref. 23. In (b) we highlight the hole pockets around $\overline{N}$ and $\overline{S}$ that have shrunk upon hydrogen adsorption. For the evolution of the electron pocket see Figs. 7 and 8. The data were measured using He $I\alpha$ radiation (21.2 eV).

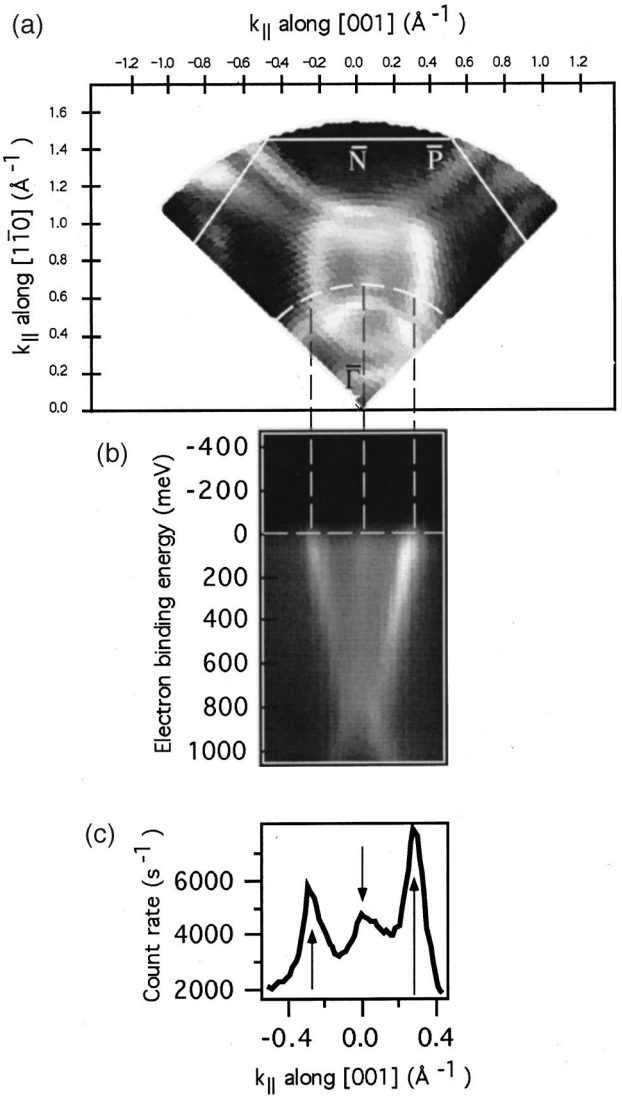

FIG. 7. (a) Sector around $\overline{N}$ for the clean surface using better statistics and an enhanced density of data points compared to Fig. 6(a). The intensity is plotted on a logarithmic scale. (b) Azimuthal angle-scanned collection of energy-distribution curves along the dashed line indicated in (a). Clearly the Fermi-level crossings can be seen and assigned to the contours of the Fermi-surface map in (a). (c) Angular distribution curve at the Fermi edge, extracted from the data set in (b). The data were measured using He $I\alpha$ radiation (21.2 eV).

and the electron pocket has expanded along the $\overline{\Gamma H}$ direction ([001]), while a bulk-related feature has not moved. This latter feature has also been observed in a recent study of Li/Mo(110).[37] As the work-function change from the clean to the hydrogen-saturated surface is ≈0.1 eV (Ref. 38) the modification of the value of $k_{\parallel}$ can be neglected.

As mentioned above we will now look at regions of the surface Brillouin zone where major changes of the Fermi-surface contours appear according to Fig. 6. For this purpose we chose the sectors around $\overline{N}$ and $\overline{S}$ as indicated in the data set of Fig. 6(a). Let us begin with the sector around $\overline{N}$ where the range of azimuthal angles covers a 90° sector symmetric around the $\overline{\Gamma N}$ direction. For the clean Mo(110) data set shown in Fig. 7(a) we applied a dwell time of 2 s and a step in the polar angle of 1°. In order to confirm that the displayed contours originate from Fermi-level crossings of electronic states we measured an azimuthal angle-scanned collection of energy-distribution curves along the dashed line indicated in Fig. 7(a). For this measurement we fixed the polar angle at 19°, resulting in a parallel wave vector of the emitted photoelectrons of ≈0.7 Å^{-1}. Each energy-distribution curve runs from 1050 to −450 meV electron binding energy in steps of 10 meV while the azimuthal angle step is chosen to be 1.5°. We have added to Fig. 7(b) a dashed line indicating the

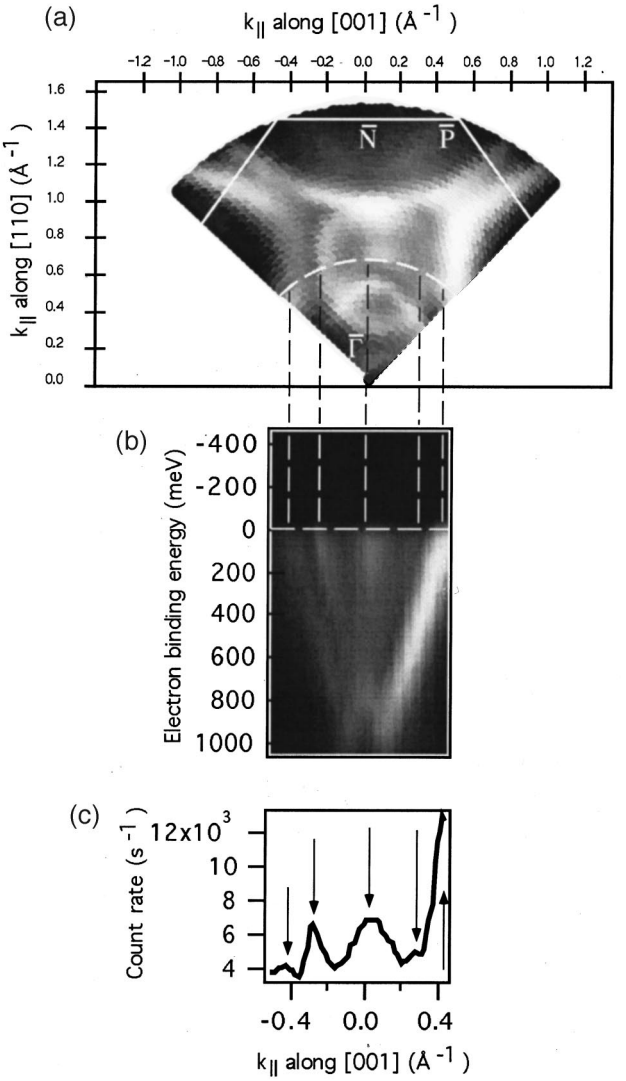

FIG. 8. Completely analogous to Fig. 7, now for the hydrogen-saturated surface. Notice that one band shifted towards the surface Brillouin-zone boundary. The azimuthal angle-scanned collection of energy-distribution curves in (b) thus shows five Fermi-level crossings instead of three: the outer ones belong to the shifted band and the remaining ones are bulk band contributions that are not affected by hydrogen adsorption.

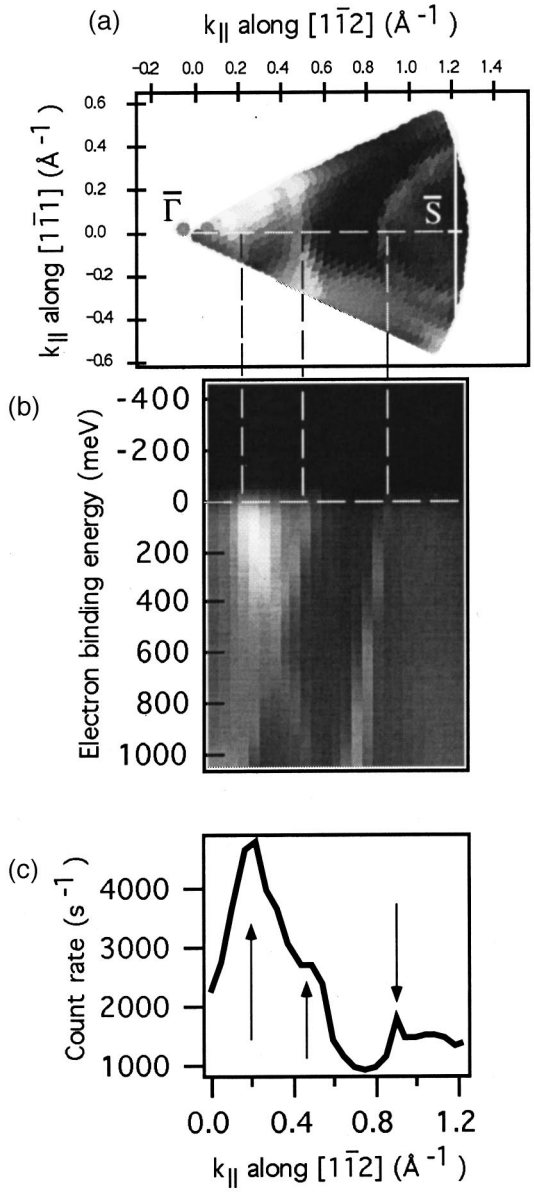

FIG. 9. (a) Sector around $\bar{S}$ for the clean surface as indicated in Fig. 6(a). Again we chose a logarithmic scale for presenting the photocurrent intensity. (b) Polar angle-scanned collection of energy-distribution curves along the dashed line shown in the sector. The Fermi-level crossings can be observed and belong to the contours demonstrated in the sector. (c) Angular distribution curve at the Fermi level from the data set in (b). The data were measured using He $I\alpha$ radiation (21.2 eV).

Fermi level. Clearly one can assign the contours measured in the data set of Fig. 7(a) to the Fermi-level crossings of the bands displayed in Fig. 7(b). Moreover, we can confirm the result of Jeong, Gaylord and Kevan[23] that the two strong Fermi-surface contours form an electron pocket, i.e., that they enclose occupied states. In order to locate the Fermi-level crossings more precisely we display in Fig. 7(c) an angular distribution curve that has been extracted from the data set of Fig. 7(b) at the Fermi edge.

These high-resolution data for the clean surface must hence be compared to the analogous results for the hydrogen-saturated surface that are displayed in Fig. 8. The hydrogen-induced changes are as follows: one band has shifted away from the $\overline{\Gamma N}$ symmetry line along the $\overline{\Gamma H}$ direction. This band, which appears twice in this data set due to the $\overline{\Gamma N}$ mirror symmetry, shows a pronounced asymmetry in the measured intensity. The appearance on the right-hand side is much stronger than on the left-hand side. This type of mirror-symmetry breaking is due to our oblique photon incidence geometry and has been observed in other cases.[39] This asymmetry being similar in the clean and H-saturated Mo(110) data indicates the common orbital symmetry of the observed states in both cases. According to Kohler *et al.*[25–28] this is the $(d_{3z^2-r^2}, d_{xy})$ band. Instead of the three Fermi-level crossings one can now distinguish five [see Fig. 8(c)]: the outermost ones belong to the H-shifted bands and the remaining bands are Fermi-level crossings of bulk electronic states that are obviously not affected by hydrogen adsorption. Notably they appear at very similar locations as the

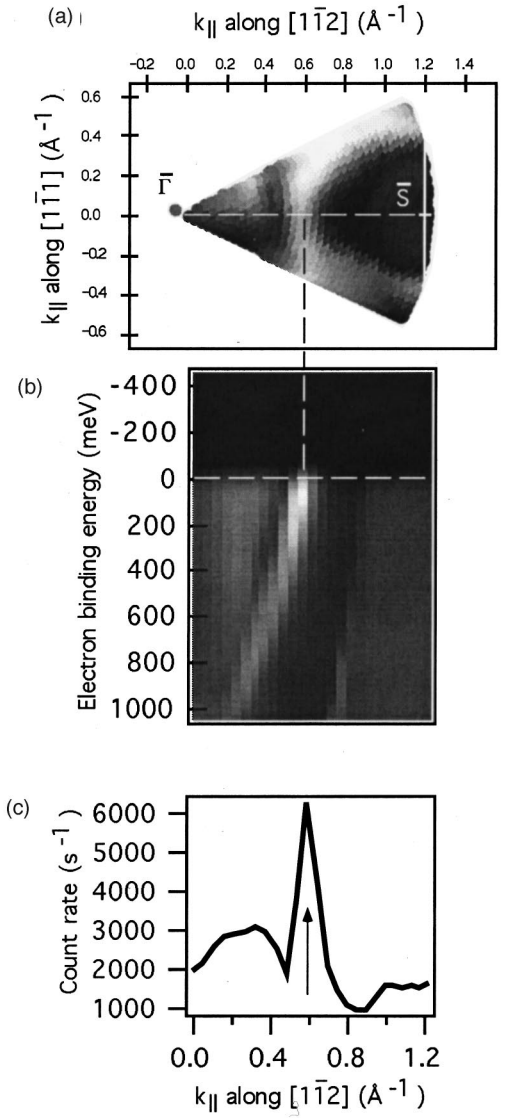

FIG. 10. Completely analogous to Fig. 9, now for the hydrogen-saturated surface. Note that the intensity of the shifted band has increased compared to the clean case.

$(d_{3z^2-r^2}, d_{xy})$ band of the clean surface.[37]

As will be discussed in more detail below, the amount of H-shifting is in very nice agreement with the calculations of Kohler *et al.*[27] In the logarithmic intensity representation of Fig. 6 we note that the hole pockets around $\bar{N}$ and $\bar{S}$ shrink considerably towards the high-symmetry points, but they do not disappear completely as had been suggested by Jeong, Gaylord, and Kevan.[23] As far as the $\bar{S}$ pocket is concerned this observed shrinking is much in agreement with the calculations by Kohler *et al.*[25–28] [see Fig. 3(c)]. For the $\bar{N}$ pocket the problem may be that in these slab calculations it is difficult to distinguish surface resonances from bulk states. Similar changes can be observed around the $\bar{S}$ point of the surface Brillouin zone as Figs. 9 and 10 suggest. The part of the complete Fermi-surface map presented here is a 50° sector symmetric around the $\bar{\Gamma}\bar{S}$ direction. We also measured polar angle-scanned collections of energy-distribution curves along the indicated line. The results are presented in Figs. 9(b) and 10(b): the electron binding-energy interval is chosen equally to the azimuthal scan data of Figs. 7(b) and 8(b); the step of the polar angle is chosen to be 1.5°. Again we find that the contours displayed in Fig. 9(a) belong to Fermi-level crossings of electronic bands, i.e., they are Fermi-surface contours, and it is confirmed that the contours surrounding $\bar{\Gamma}$ and $\bar{S}$ are hole pockets whereas the remaining contour is an electron pocket. In Fig. 9(c) we give an angular distribution curve at the Fermi edge [notice the horizontal dashed line in Fig. 9(b)] which allows for precisely locating the Fermi-level crossings.

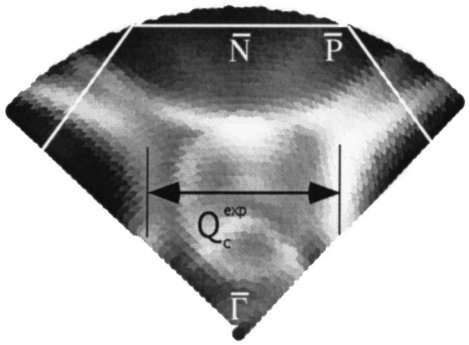

FIG. 11. Quasi-one-dimensional Fermi-surface nesting along the $\bar{\Gamma}\bar{H}$ direction ([001]). The corresponding nesting vector $\mathbf{Q}_c^{\exp}$ is included and is in agreement with the wave vector of the anomalous phonon modes along this direction. The intensity is plotted on a logarithmic scale.

On the H-saturated surface (Fig. 10), the Fermi-surface contour that belongs to the electron pocket shifts towards the zone boundary and increases its intensity markedly. Again the amount of shifting is in very good agreement with the theoretical results (see below). As already discussed above, the hole pocket around $\bar{S}$ does not vanish in our data, i.e., we do not observe a complete filling of the associated band upon H saturation. Rather, we observe a shift towards the $\bar{S}$ point, in good agreement with the calculations by Kohler *et al.*[25–28]

We reexamine now the data sets from the H-saturated surface of Figs. 8 and 10 in terms of Fermi-surface nesting. In Fig. 11 we display again the sector around $\bar{N}$ and draw the attention to the nested regions of the Fermi-surface contours. The white and the black lines serve as guides to the eye. Obviously the electron pocket contours possess large parallel parts and consequently one can qualify this situation as quasi-one-dimensional Fermi-surface nesting. More importantly, the length of the included nesting vector $\mathbf{Q}_c^{\exp}$ as derived most precisely from Fig. 8(c) is $|\mathbf{Q}_c^{\exp}| = 0.85\,\text{Å}^{-1}$, which is in excellent agreement with both the theoretical and the experimental value obtained by vibrational spectroscopy. Figure 12 is dedicated to the sector around $\bar{S}$. Inversion symmetry was exploited in order to add the lower part of this Fermi-surface map. Again we extract the length of the indicated nesting vector from Fig. 10(c) and obtain $|\mathbf{Q}_c^{\exp}| = 1.19\,\text{Å}^{-1}$ which compares very well with the calculated value[27] and with the result from vibrational spectroscopy (the reader is referred to Table I where in the fourth column we added our results on the critical wave vectors). In this context it is interesting to cite a recently published paper investigating the Fermi-level crossings of hydrogen-saturated W(110) where similar phonon anomalies have been ob-

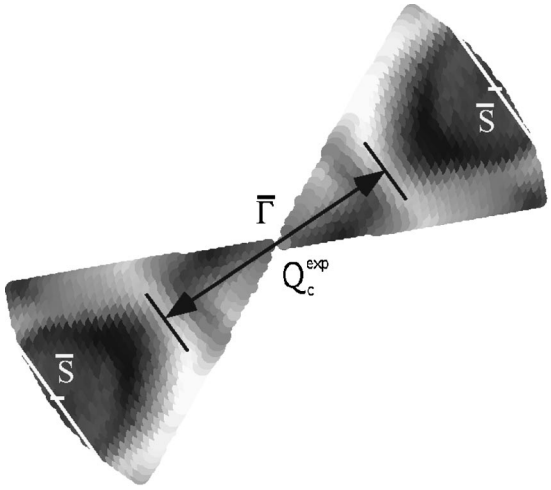

FIG. 12. Quasi-one-dimensional Fermi-surface nesting along the $\overline{\Gamma S}$ direction ($[1\bar{1}2]$). The lower part of the Fermi-surface map results from the upper part by exploiting inversion symmetry. The corresponding nesting vector $\mathbf{Q}_c^{exp}$ is included and is in agreement with the wave vector of the anomalous phonon modes along this direction. The intensity of the photocurrent is presented on a logarithmic scale.

served. Rotenberg and Kevan[40] demonstrate that here the nesting takes place between spin-orbit split surface bands. In the case of Mo(110) we have not found any hint for spin-orbit split contours, i.e., we can account for all observed contours either by surface states of bulk bands. For this substrate the spin-orbit interaction is less important than for tungsten and consequently a splitting of contours should not be expected.

In the following we would like to address two more things. Firstly, from our photoemission data no hint can be extracted why for the clean surface the dispersion curve for the longitudinal mode is lowered towards the Brillouin-zone boundary along $\overline{\Gamma N}$. Specifically, we find no nested regions of Fermi-surface contours that could explain the lowering in terms of a Kohn anomaly. Secondly, the reader is reminded that the phonon anomaly sets in before saturation of the surface with hydrogen is accomplished, i.e., the energies of the phonon modes are slightly lowered (see Fig. 2) for coverages below 1 ML. From the point of view of the photoemission experiment we were thus interested to reveal the gradual changes of the Fermi-surface contours with increasing hydrogen exposure. We examined the sector around the $\bar{N}$ point in order to observe the development of the contours. The first data set [Fig. 13(a)] is the already known Fermi-surface map for the clean surface at room temperature. Figure 13(b) reveals the contours after exposing the sample to a hydrogen atmosphere of 5×10^{-7} Pa for 90 s, which corresponds to $\approx$0.6 L, taking into account a sensitivity factor of 1.6 for the Bayard-Alpert ion gauge (1 L=1 Langmuir=10^{-6} Torr s). One can observe that already after this small exposure to hydrogen the hole pocket around $\bar{N}$ becomes smaller and the contour of the electron pocket begins its way along $\overline{\Gamma H}$ towards the $\bar{H}$ point. After 1.5 L hydrogen exposure [see Fig. 13(c)] the hole pocket has further decreased in size and one can see now that the contour of the electron pocket starts to seperate from the weaker bulk band, which is unaffected by

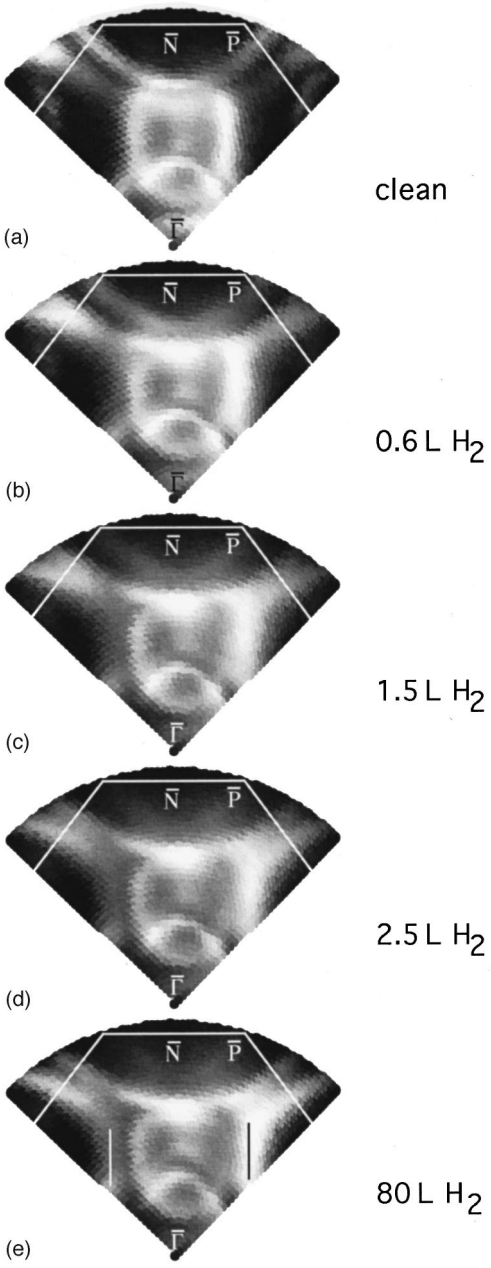

FIG. 13. Development of the Fermi-level crossings with increasing hydrogen coverage. Starting from the clean surface (upper data set) the Fermi-surface maps for hydrogen exposures of 0.6, 1.5, 2.5, and 80 L are shown. Notice the strong similarity between the last two data sets. In all data sets we used a logarithmic scale for the intensity of the photocurrent.

hydrogen adsorption.[37] This separation can be seen more clearly after an exposure of 2.5 L [Fig. 13(d)]. Here the hole pocket around $\bar{N}$ has nearly vanished. It is interesting that the contours at 2.5 L are very similar to the contours recorded after 80 L hydrogen exposure [Fig. 13(e)]. Especially the nested regions of the Fermi contours as indicated by the white and black lines in Fig. 13(e) are already developed at 2.5 L. Notice that the electron-energy-loss spectroscopy experiment[17,18] reports the beginning phonon anomaly at 0.75 ML which was achieved with $\approx$3 L of hydrogen exposure. In order to compare the hydrogen exposures of the present experiment with those of the former vibrational spec-

troscopy analysis we performed a low-energy electron diffraction experiment where we observed the development of the diffraction pattern during hydrogen adsorption. Since a (2×2) superstructure exists for coverages between 0.5 and 0.75 MI (Refs. 17 and 31) it was possible to compare the hydrogen-exposure values directly, resulting in good agreement. The main difference seems to be the intensity of the electron pocket contour which is larger for the saturated surface. In other words, the same nesting vector along $\overline{\Gamma H}$ (the data for the $\overline{\Gamma S}$ is analogous but not shown here) exists for the Fermi-surface contours after 2.5 L hydrogen exposure and it should thus be responsible for the beginning phonon anomaly. The question remains open why the anomaly is not fully developed at this coverage although the Fermi-surface nesting is obviously the same as for saturation. This question leads to the prerequisites that must be fulfilled for a giant Kohn anomaly in general and it seems appropriate to discuss the character of this anomaly a bit more thoroughly. It belongs to textbook physics[41] that a free electron gas redistributes its charge density in the presence of a positive charge in order to cancel out the long-range Coulombic field of the positive charge. In a solid a phonon mode can be viewed as a positive charge density neglecting its discrete character which is screened by the conduction electrons. This situations leads to a reduction of the long-range interaction of the ions which can be quantified by the dielectric constant of the electron gas. In the same way as the force between the ions is reduced by the dielectric constant so is the phonon frequency. Using the Lindhard dielectric function one can calculate the amount of this reduction. Kohn pointed out that the singularity of the Lindhard dielectric function at a wave vector of $2k_F$ (k_F being the Fermi wave vector) should be visible in phonon dispersion curves in form of kinks.[42] Especially in one dimension these kinks are developed to the full extent, i.e., the phonon-dispersion curve drops down to zero energy at $2k_F$, which corresponds to a static reconstruction of the one-dimensional linear ion chain. This effect is better known as the Peierls distortion.[43] For a one-dimensional system the Fermi surface consists of two parallel planes with a distance of $2k_F$ in reciprocal space and many electrons can thus take part in the anomalous phonon softening. In our case the one-dimensional situation is not completely restored but there exist large parts of nested regions of the Fermi contours that make the situation quasi-one-dimensional. This is the reason why the anomaly is called a *giant* Kohn anomaly. As a result of our investigation we must assert that the existence of nested regions of Fermi-surface contours is necessary but not sufficient for a giant Kohn anomaly.

What other requirements apart from the existence of nested Fermi contours must be fulfilled in order to drive a phonon anomaly? At the present state we can only speculate why the nested Fermi-surface contours already exist below saturation although the surface phonon anomaly has not fully developed. One reason might be that the matrix elements responsible for the coupling strength between electronic and nuclear systems, considered as a function of the hydrogen coverage, might reach their maximum at saturation. This would lead to a minor interaction for coverages below saturation and could explain our observations.[44] Another reason could be that our experiment was performed at room temperature. Thus the ordering of the adsorbate structure should not be as perfect as for the cooled surface that was investigated by vibrational spectroscopy.[14–18] Locally, hydrogen-saturated patches might therefore be expected on the room-temperature surface that contributes to the observed Fermi-surface contours, but which are not large enough to support the softened phonon modes.

IV. SUMMARY AND CONCLUSION

We have investigated the Fermi-level crossings for clean and hydrogen-saturated Mo(110) using angle-resolved photoelectron spectroscopy. Moreover, we have measured in detail the development of Fermi-surface contours with increasing hydrogen coverage for parts of the surface Brillouin zone. In our data we clearly observe quasi-one-dimensional Fermi-surface nesting for the hydrogen-saturated surface. The corresponding nesting vectors are in excellent agreement with the wave vectors of surface phonon modes that are anomalously lowered in energy as observed by experiments using the inelastic scattering of He atoms[14–16] and electrons[17,18] and as calculated from density-functional theory.[25–28] Consequently, the existing discrepancy between theory and a previous photoemission experiment on this system could be resolved in favor of the theoretical calculations. We conclude that the observed adsorbate-induced phonon anomaly is a giant Kohn anomaly due to quasi-one-dimensional Fermi-surface nesting. Furthermore, we can deduce from our experiment that the nesting property alone need not cause a fully developed phonon anomaly. Another prerequisite may be a sufficiently large coupling between electrons and ions in order to transfer the electronic instability to the observed lattice instability.

ACKNOWLEDGMENTS

We would like to thank U. Linke for preparing the molybdenum crystal and H. Ibach for kindly placing the crystal at our disposal. We appreciate the help of P. Aebi concerning the construction of a sample holder which allows for heating the crystal to 2000 K. The authors want to thank W. Deichmann for his support and the mechanical workshop for technical assistance. This work has been supported by the Swiss National Foundation.

[1] B. M. Powell, P. Martell, and A. D. B. Woods, Phys. Rev. **171**, 727 (1968).
[2] C. M. Varma and W. Weber, Phys. Rev. B **19**, 6142 (1979).
[3] C. M. Varma and W. Weber, Phys. Rev. B **39**, 1094 (1977).
[4] J. Zarestky, C. Stassis, B. N. Harmon, K.-M. Ho, and C.-L. Fu, Phys. Rev. B **28**, 697 (1983).
[5] D. Singh and H. Krakauer, Phys. Rev. B **43**, 1441 (1991).
[6] Y. Chen, C.-L. Fu, K.-M. Ho, and B. N. Harmon, Phys. Rev. B **31**, 6775 (1985).
[7] K.-M. Ho, C.-L. Fu, and B. N. Harmon, Phys. Rev. B **29**, 1575

(1984).
[8] C.-L. Fu, K.-M. Ho, and B. N. Harmon, Phys. Rev. B **28**, 2957 (1983).
[9] K.-M. Ho, C.-L. Fu, B. N. Harmon, W. Weber, and D. R. Hamann, Phys. Rev. Lett. **49**, 673 (1982).
[10] P. J. Estrup, Surf. Sci. **299/300**, 722 (1994).
[11] T. E. Felter, R. A. Barker, and P. J. Estrup, Phys. Rev. Lett. **38**, 1138 (1977).
[12] E. Hulpke and D.-M. Smilgies, Phys. Rev. B **40**, 1338 (1989).
[13] J. W. Chung, K.-S. Shin, D. H. Baek, C. Y. Kim, S. K. Lee, C. Y. Park, S. C. Hong, T. Kinoshita, M. Watanabe, A. Kakizaki, and T. Ishii, Phys. Rev. Lett. **69**, 2228 (1992).
[14] E. Hulpke and J. Lüdecke, Surf. Sci. **287/288**, 837 (1993).
[15] E. Hulpke and J. Lüdecke, J. Electron Spectrosc. Relat. Phenom. **64/56**, 641 (1993).
[16] E. Hulpke, in *Electronic Surface and Interface States on Metallic Systems*, edited by E. Berthel and M. Donath (World Scientific, Singapore, 1995).
[17] J. Kröger, S. Lehwald, and H. Ibach, Phys. Rev. B **55**, 10 895 (1997).
[18] J. Kröger, Ph.D. dissertation, Rheinisch-Westfälische Technische Hochschule Aachen, D 82, 1998.
[19] S. D. Kevan, in *Elecronic Surface and Interface States on Metallic Systems*, edited by E. Bertel and M. Donath (World Scientific, Singapore, 1995).
[20] S. D. Kevan, Surf. Sci. **307–309**, 332 (1994).
[21] R. H. Gaylord, K. Jeong, and S. D. Kevan, Phys. Rev. Lett. **62**, 2036 (1989).
[22] K. Jeong, R. H. Gaylord, and S. D. Kevan, J. Vac. Sci. Technol. A **7**, 2199 (1989).
[23] K. Jeong, R. H. Gaylord, and S. D. Kevan, Phys. Rev. B **39**, 2973 (1989).
[24] K. Jeong, R. H. Gaylord, and S. D. Kevan, Phys. Rev. B **38**, 10 302 (1988).
[25] B. Kohler, P. Ruggerone, and M. Scheffler, Surf. Sci. **368**, 108 (1996).
[26] B. Kohler, P. Ruggerone, M. Scheffler, and E. Tosatti, Z. Phys. Chem. (Munich) **197**, 193 (1996).
[27] B. Kohler, P. Ruggerone, S. Wilke, and M. Scheffler, Phys. Rev. Lett. **74**, 1387 (1995).
[28] B. Kohler, Ph.D. dissertation, Technische Universität Berlin, D 83, 1995.
[29] M. Altman, J. W. Chung, P. J. Estrup, J. M. Kosterlitz, J. Prybyla, D. Sahu, and S. C. Ying, J. Vac. Sci. Technol. A **5**, 1045 (1987).
[30] M. Okada, A. P. Baddorf, and D. M. Zehner, Surf. Sci. **373**, 145 (1997).
[31] M. Arnold, S. Sologub, W. Frie, L. Hammer, and K. Heinz, J. Phys.: Condens. Matter **9**, 6481 (1997).
[32] M. Arnold, S. Sologub, G. Hupfauer, P. Bayer, W. Frie, L. Hammer, and K. Heinz, Surf. Rev. Lett. **4**, 1291 (1997).
[33] T. Greber, O. Raetzo, T. J. Kreutz, P. Schwaller, W. Deichmann, E. Wetli, and J. Osterwalder, Rev. Sci. Instrum. **68**, 4549 (1997).
[34] J. Osterwalder, Surf. Rev. Lett. **4**, 391 (1997).
[35] T. J. Kreutz, T. Greber, P. Aebi, and J. Osterwalder, Phys. Rev. B **58**, 1300 (1998).
[36] D. A. Papaconstantopoulos, *Handbook of the Band Structure of Elemental Solids* (Plenum, New York, 1986).
[37] E. Rotenberg, J. W. Chung, and S. D. Kevan, Phys. Rev. Lett. **82**, 4066 (1999).
[38] R. Liu and G. Ehrlich, Surf. Sci. **119**, 207 (1982).
[39] J. Osterwalder, T. Greber, P. Aebi, R. Fasel, and L. Schlapbach, Phys. Rev. B **53**, 10 209 (1996).
[40] E. Rotenberg and S. D. Kevan, Phys. Rev. Lett. **80**, 2905 (1998).
[41] N. W. Ashcroft and N. D. Mermin, *Solid State Physics* (Saunders, Philadelphia, 1976).
[42] W. Kohn, Phys. Rev. Lett. **2**, 393 (1959).
[43] R. E. Peierls, *Quantum Theory of Solids* (Clarendon, Oxford, 1955).
[44] M. Scheffler (private communication).